Electronic Supplementary Material (ESI) for Soft Matter.

Supporting Information

Fractal-Inspired Soft Deployable Structure: A Theoretical Study

Zechen Xiong[1], Hang Xiao[2,*] and Xi Chen[1,*]

[1]*Earth Engineering Center, Center for Advanced Materials for Energy and Environment, Department of Earth and Environmental Engineering, Columbia University, New York, NY 10027, USA*

[2]*School of Chemical Engineering, Northwest University, Xi'an 710069, China*

Comparison between beam theories

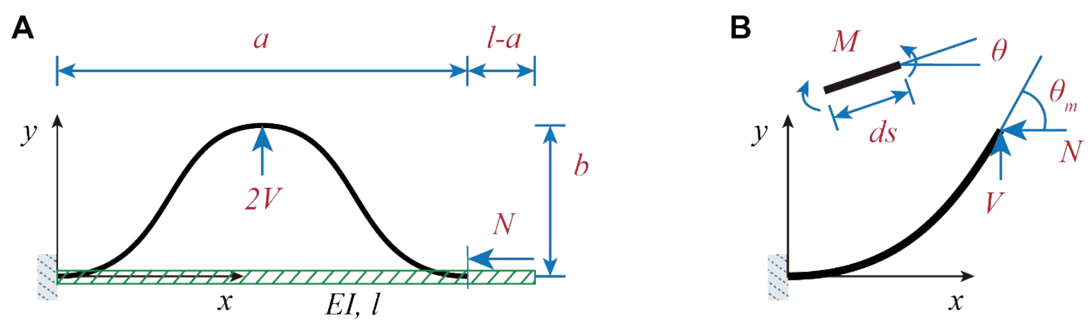

Fig. S1 A double clamped beam subjected to midway shearing and end compressive load. (A) The force diagram of the beam. (B) A quarter of the beam and the denotations.

This section shows the kinematics of a beam structure under two principal deformation patterns: compressive buckling and shearing, using large deflection beam theory, and further comparing the results with conventional beam theories.

Assuming the membrane strain of the fixed-fixed beam in Fig. S1 is negligible compared to the bending strain (since the membrane stiffness of such thin-wall structure is much larger than the bending stiffness), i.e. the total arc length of the beam doesn't change, the Euler-Bernoulli theory considering large rotation gives:

$$M = EI\frac{d\theta}{ds} = EI\frac{\frac{d^2y}{dx^2}}{\left(1+\left(\frac{dy}{dx}\right)^2\right)^{\frac{3}{2}}} \qquad \text{* MERGEFORMAT (1)}$$

According to equilibrium, the internal moment at any point in the beam is given by

$$M = N\left(\frac{b}{2}-y\right)+V\left(\frac{a}{4}-x\right) \qquad \text{* MERGEFORMAT (2)}$$

Combining eq. (1) and eq. (2), the curvation may be rewritten as

* Corresponding author, xichen@columbia.edu (X. Chen); xiaohang07@nwu.edu.cn (H. Xiao)

$$\frac{d\theta}{ds}=\frac{N}{EI}\left(\frac{b}{2}-y\right)+\frac{V}{EI}\left(\frac{a}{4}-x\right) \qquad \text{* MERGEFORMAT (3)}$$

To consider the compressive buckling case, we consider the scenario where V=0, i.e. where beam only subjected to horizontal loads, thus

$$\frac{d^2\theta}{ds^2}=\frac{N}{EI}\left(-\frac{dy}{ds}\right)=-\frac{N}{EI}\sin\theta \qquad \text{* MERGEFORMAT (4)}$$

Integration yields:

$$\frac{1}{2}\left(\frac{d\theta}{ds}\right)^2=\frac{N}{EI}\cos\theta+C_1 \qquad \text{* MERGEFORMAT (5)}$$

Considering the boundary condition at the inflection point where $\theta=\theta_m$ and $d\theta/ds=0$, C_1 is obtained as

$$C_1=\frac{-N}{EI}\cos\theta_m \qquad \text{* MERGEFORMAT (6)}$$

Substituting eq. (6) into eq. (5) yields

$$\frac{d\theta}{ds}=\sqrt{2}\sqrt{\frac{N}{EI}}\sqrt{-\cos\theta_m+\cos\theta} \qquad \text{* MERGEFORMAT (7)}$$

And the equation can be transformed to

$$\alpha=4F\left(\frac{\pi}{2},k\right)=4F(k) \qquad \text{* MERGEFORMAT (8)}$$

where

$$\alpha=\sqrt{\frac{Nl^2}{EI}},\ k=\sqrt{\frac{-\cos\theta_m+1}{2}}$$

and $F(\phi,k)$ is an incomplete elliptical integral of the first kind defined as

$$F(\phi,k)=\int_0^{\phi}\frac{d\theta}{\sqrt{1-k^2\sin^2\theta}}$$

When θ_m=0, the solution degenerate to

$$N_{cr}=\frac{4\pi^2 EI}{l^2} \qquad \text{* MERGEFORMAT (9)}$$

which corresponds with Euler's critical load. Otherwise, the load is derived as

$$N_{post-cr}=\frac{16F(k)^2 EI}{l^2} \qquad \text{* MERGEFORMAT (10)}$$

Similarly, the horizontal contraction and transverse deflection of the clamped-clamped beam can be expressed in elliptical integral:

$$\frac{a}{l}=\frac{2E(k)}{F(k)}-1 \qquad \text{* MERGEFORMAT (11)}$$

$$\frac{b}{l}=\frac{k}{F(k)} \qquad \text{* MERGEFORMAT (12)}$$

where $E(\phi,k)$ is an incomplete elliptical integral of the second kind, defined as

$$E(\phi,k)=\int_0^{\phi}\sqrt{1-k^2\sin^2\theta}\,d\theta$$

From eq. (1) and eq. (3), relations between θ and s can be rewritten as

$$\frac{M}{EI}=\frac{\alpha^2}{l^2}\left(\frac{b}{2}-y\right)=\frac{d\theta}{ds}=\frac{\sin\theta d\theta}{dy} \qquad \text{* MERGEFORMAT (13)}$$

Separating variables and integrating yield

$$\cos\theta=1-\alpha^2\left(\frac{b}{2l^2}y-\frac{1}{2l^2}y^2\right) \qquad \text{* MERGEFORMAT (14)}$$

whose constant of integration can be derived from the boundary condition at the encastred end, where $y = 0$ and θ=0. Eliminating θ by substituting dx=cotθ·dy into eq. (14), the profile of the post-buckling beams under specific compressing load can be expressed as the integration of a transcendental function

$$\begin{cases}\dfrac{x}{l}=\displaystyle\int_0^{y/l}\cot\cos^{-1}\left(1-\alpha^2\left(\frac{1}{2}\frac{b}{l}t-\frac{1}{2}t^2\right)\right)dt, & 0\le\dfrac{y}{l}\le\dfrac{b}{l}\\ \dfrac{x}{l}=\dfrac{a}{l}-\displaystyle\int_0^{y/l}\cot\cos^{-1}\left(1-\alpha^2\left(\frac{1}{2}\frac{b}{l}t-\frac{1}{2}t^2\right)\right)dt, & 0<\dfrac{y}{l}\le\dfrac{b}{l}\end{cases} \qquad \text{* MERGEFORMAT}$$

(15)

Applying the same principles, we can obtain for the "pure shearing" case where N=0 that

$$\begin{cases}\alpha=4(F(k)-F(t_0,k))\\ \dfrac{a}{l}=\dfrac{8k\cos t_0}{\alpha}=\dfrac{4\sqrt{2}}{\alpha}\sqrt{\sin\theta_m}\\ \dfrac{b}{l}=\dfrac{2}{\alpha}\left(F(k)-F(t_0,k)-2\left(E(k)-E(t_0,k)\right)\right)=\dfrac{1}{2}-\dfrac{4}{\alpha}\left(E(k)-E(t_0,k)\right)\end{cases} \qquad \text{* MERGEFORMAT (16)}$$

and

$$\begin{cases} \dfrac{y}{l} = \displaystyle\int_0^{x/l} \tan\left(\sin^{-1}\alpha^2\left(\frac{a}{4l}t - \frac{1}{2}t^2\right)\right)dt, & 0 \le \dfrac{x}{l} \le \dfrac{a}{2l} \\ \dfrac{y}{l} = \displaystyle\int_0^{a/l - x/l} \tan\left(\sin^{-1}\alpha^2\left(\frac{a}{4l}t - \frac{1}{2}t^2\right)\right)dt, & \dfrac{a}{2l} \le \dfrac{x}{l} \le \dfrac{a}{l} \end{cases} \quad \text{* MERGEFORMAT (17)}$$

where

$$k = \sqrt{\frac{1+\sin\theta_m}{2}}, t_0 = \sin^{-1}\sqrt{\frac{1}{2k^2}}$$

and the non-dimensional load

$$\alpha = \sqrt{\frac{Vl^2}{EI}}$$

Detailed derivations of the above process can also be referred to in the literature[1–3]. Though original functions can not be found for the integrants in eq. (15) and eq. (16), their integrations are readily calculable using numerical software. And their comparisons with small deflection profile solution ($A\sin(k)+Ax$ and polynomial), quadratic trigonometric approximation ($A\sin^2(kx)$)[4,5], and finite-element (FE) results are shown in Fig. S2. While the quadratic trigonometric method gives results corresponding to the FE outcome, with a maximum error of ca. 10%, the small deflection results can be divergent. Meanwhile, the large deflection theory has a very small error of ca. 0.1%, verifying its accuracy. A more general closed-form solution of double clamped beams subjected to arbitrary loads can be referred to in the literature[6], in which the conclusions obtained above still apply.

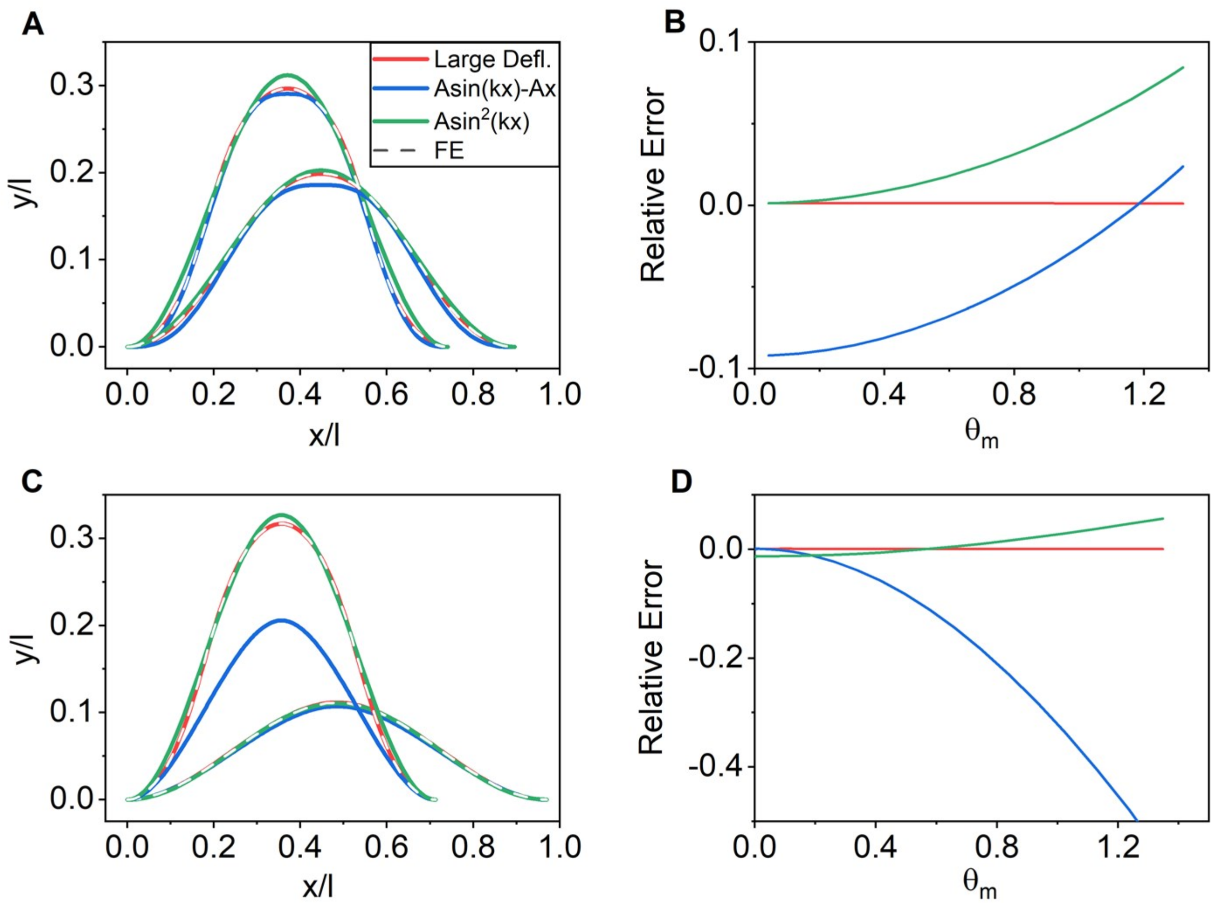

Fig. S2 The profile comparison and relative error of different beam theory. (A) and (C) show the normalized beam profile under compressive buckling and "pure shearing", respectively. Maximum rotation θ_m=π/2 and 0.65 cases are included for both. (B) and (D) give the relative errors compared to the FE results as a function of θ_m.

Implementation Methods

While detailed fabrication techniques and material usage for fractal-inspired soft deployable (FISD) structures are beyond the scope of this work, one of the possible implementation schemes can be envisioned based on experience, literature[7–10], and representative designs in Fig. 1. Using a high-resolution 3D printer (Objet260 Connex3, Stratasys, ±0.1 mm accuracy and 16-micron layer thickness) and Vero photopolymers (2-3 GPa elastic modulus, 25% maximum elongation) as matrix material, a thin-walled honeycomb prototype with 12 representative volume elements (RVE, blue square in Fig. 1C) can be built as shown in Fig. S3. While the thickness of each thin-walled beam remains as 0.6 mm, the slits between them have a height of h = 0.2 mm to keep a clearance, and the height of central slits (Fig. S3B) of each RVE is given as h_0 = 1.0 mm to install the actuation (shape-memory coil actuator[9,11,12] denoted by red dotted line in Fig. S3B, while highly swellable hydrogels can also be an applicant[7,13,14]). Including the rigid clamps attached (5×5 mm^2, blue regions in Fig. S3A) at both ends, the FISD honeycomb planar actuator has a total dimension of 246× 41.1×5 mm^3. Necessary modifications in the fabrication and assembly processes may have an impact on the detailed configurations.

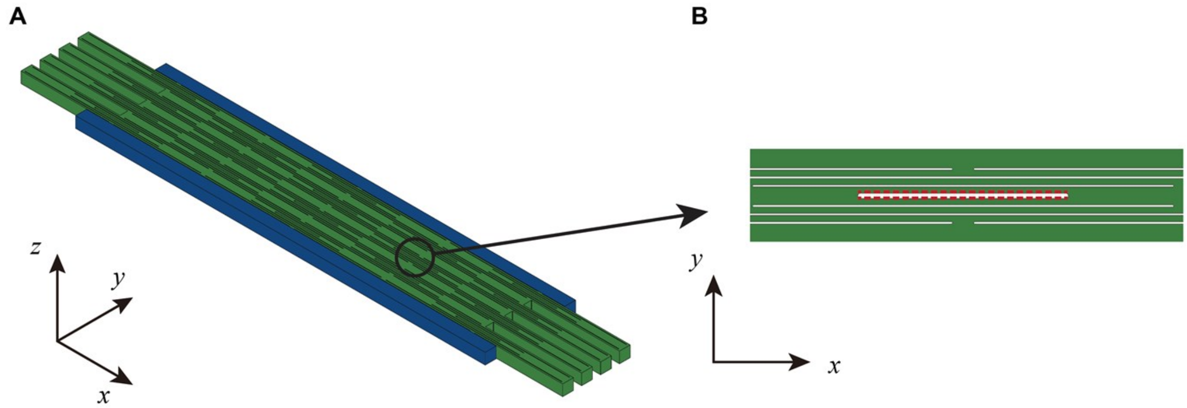

Fig. S3 The implementation scheme for the FISD structures using a high-resolution 3D printer and SMA. (A) shows the assumed prototype consisting of an FISD honeycomb (green) and rigid clamps attached at the ends (blue). (B) presents the configuration of the central slits with SMA coils (red dotted line) installed.

References

1 L. L. Howell and A. Midha, *J. Mech. Des.*, 1995, **117**, 156.

2 C. Kimball and L.-W. Tsai, *J. Mech. Des*, 2002, **124**, 223–235.

3 P. F. Byrd and M. D. Friedman, *Handbook of elliptic integrals for engineers and physicists*, Springer; Lange, Maxwell & Springer, Berlin; New York, 1954.

4 Y. Su, J. Wu, Z. Fan, K.-C. Hwang, J. Song, Y. Huang and J. A. Rogers, *Journal of the Mechanics and Physics of Solids*, 2012, **60**, 487–508.

5 Y. Shi, P. Pei, X. Cheng, Z. Yan, M. Han, Z. Li, C. Gao, J. A. Rogers, Y. Huang and Y. Zhang, *Soft Matter*, 2018, **14**, 8828–8837.

6 Y. Zhang, Y. Jiao, J. Wu, Y. Ma and X. Feng, *Extreme Mechanics Letters*, 2020, **34**, 100604.

7 L. Guiducci, K. Razghandi, L. Bertinetti, S. Turcaud, M. Rüggeberg, J. C. Weaver, P. Fratzl, I. Burgert and J. W. C. Dunlop, *PLoS One*, , DOI:10.1371/journal.pone.0163506.

8 Z. Ding, C. Yuan, X. Peng, T. Wang, H. J. Qi and M. L. Dunn, *Science Advances*, 2017, **3**, e1602890.

9 N. An, M. Li and J. Zhou, *International Journal of Mechanical Sciences*, 2020, **180**, 105753.

10Y. Li, Y. Chen, T. Li, S. Cao and L. Wang, *Composite Structures*, 2018, **189**, 586–597.

11 Huai-Ti Lin, Gary G. Leisk, and Barry Trimmer, *Bioinspir. Biomim.*, 2011, **6**, 026007.

12 W. Wang, C. Li, H. Rodrigue, F. Yuan, M.-W. Han, M. Cho and S.-H. Ahn, *Advanced Functional Materials*, 2017, **27**, 1604214.

13 M. J. Harrington, K. Razghandi, F. Ditsch, L. Guiducci, M. Rueggeberg, J. W. C. Dunlop, P. Fratzl, C. Neinhuis and I. Burgert, *Nat Commun*, 2011, **2**, 337.

14 K. Razghandi, L. Bertinetti, L. Guiducci, J. W. C. Dunlop, P. Fratzl, C. Neinhuis and I. Burgert, *Bioinspired, Biomimetic and Nanobiomaterials*, 2014, **3**, 169–182.